Biochimica et Biophysica Acta 1827 (2013) 484–492

Contents lists available at SciVerse ScienceDirect

Biochimica et Biophysica Acta

journal homepage: www.elsevier.com/locate/bbabio

Solution structure of a mutant of the triheme cytochrome PpcA from *Geobacter sulfurreducens* sheds light on the role of the conserved aromatic residue F15

Joana M. Dantas [a], Leonor Morgado [a], P. Raj Pokkuluri [b], David L. Turner [c], Carlos A. Salgueiro [a,*]

[a] *Requimte-CQFB, Departamento de Química, Faculdade de Ciências e Tecnologia, Universidade Nova de Lisboa, Campus Caparica, 2829-516 Caparica, Portugal*
[b] *Biosciences Division, Argonne National Laboratory, Argonne, IL 60439, USA*
[c] *Instituto de Tecnologia Química e Biológica, Universidade Nova de Lisboa, Av. da Republica (EAN), 2780-157 Oeiras, Portugal*

ARTICLE INFO

Article history:
Received 17 October 2012
Received in revised form 11 December 2012
Accepted 14 December 2012
Available online 8 January 2013

Keywords:
Geobacter
Multiheme cytochromes
NMR
Structure–function
Site-directed mutagenesis

ABSTRACT

Extracellular electron transfer is one of the physiological hallmarks of *Geobacteraceae*. Most of the *Geobacter* species encode for more than 100 *c*-type cytochromes which are, in general, poorly conserved between individual species. An exception to this is the PpcA family of periplasmic triheme *c*-type cytochromes, which are the most abundant proteins in these bacteria. The functional characterization of PpcA showed that it has the necessary properties to couple electron/proton transfer, a fundamental step for ATP synthesis. The detailed thermodynamic characterization of a PpcA mutant, in which the strictly conserved residue phenylalanine 15 was replaced by leucine, showed that the global redox network of cooperativities among heme groups is altered, preventing the mutant from performing a concerted electron/proton transfer. In this work, we determined the solution structure of PpcA F15L mutant in the fully reduced state using NMR spectroscopy by producing ^{15}N-labeled protein. In addition, pH-dependent conformational changes were mapped onto the structure. The mutant structure obtained is well defined, with an average pairwise root-mean-square deviation of 0.36 Å for the backbone atoms and 1.14 Å for all heavy atoms. Comparison between the mutant and wild-type structures elucidated the contribution of phenylalanine 15 in the modulation of the functional properties of PpcA.

1. Introduction

Geobacter species are among the most effective microorganisms for the bioremediation of radioactive and toxic metals in contaminated subsurface environments, and for converting waste organic matter and renewable biomass to electricity [1–6]. Insoluble oxides of metals such as Fe(III), Mn(IV), U(VI), and graphite electrodes are examples of extracellular electron acceptors that can be used by *Geobacter* species [7–11]. The ability to use extracellular terminal electron acceptors presents the bacterium with additional challenges compared to microorganisms without this capability. The first challenge is to assure electron delivery to cell exterior and the second is to achieve a net production of metabolic energy that supports cellular growth. To address these challenges, *Geobacter* species present particular respiratory chains, which allow the transmembrane transfer of electrons from oxidation of organic compounds in the cytoplasm to the outside of the cells. These chains rely on a particular topology that includes inner respiratory enzymes (such as NADH and succinate dehydrogenases), periplasmic and outer-membrane cytochromes [6]. Several *c*-type cytochromes have been shown to be essential for Fe(III) reduction in *Geobacter sulfurreducens* [10,12–17]. Nonetheless, the mechanisms underlying the electron transfer towards extracellular electron acceptors are still poorly understood [8,18]. Among these electron transporters, the periplasmic triheme PpcA from *G. sulfurreducens* is the best studied protein to date, being crucial in bridging the electron transfer from cytoplasm to cell exterior when the bacteria grows in presence of U(VI) or Fe(III) oxides [8,10,11]. The triheme cytochrome PpcA is a member of the c_7 family, from which 25 members have been identified to date (for a review see [19]). The three heme groups form the protein core and each heme is covalently linked to cysteine residues of the CXXCH binding motifs (where X corresponds to any amino acid). The sequence alignment of all cytochromes c_7 showed that, among 21 highly conserved residues, only nine are not cysteine or histidine residues directly involved in heme binding. Phe^{15} is the only aromatic residue strictly conserved in the cytochrome c_7 family; it is located in a hydrophobic region between hemes I and III, with the aromatic ring almost parallel to the ring plane of heme I and perpendicular to heme III [19]. The spatial arrangement of the heme groups in c_7 cytochromes is superimposable with the structurally homologous tetraheme cytochromes c_3, with the sole difference in the absence of heme II and corresponding polypeptide segment in the c_7 family. For this reason, the three heme groups in cytochromes c_7 are

Abbreviations: PpcA, *Geobacter sulfurreducens* triheme cytochrome encoded by gene GSU0612; PpcAF15L, PpcA mutant with residue F15 replaced by leucine; rmsd, root-mean-square deviation

* Corresponding author. Tel.: +351 21 294 83 00; fax: +351 21 294 83 85.
E-mail address: csalgueiro@fct.unl.pt (C.A. Salgueiro).

0005-2728/$ – see front matter © 2013 Elsevier B.V. All rights reserved.
http://dx.doi.org/10.1016/j.bbabio.2012.12.008

numbered I, III, and IV. The functional characterization of PpcA showed that the protein has the necessary thermodynamic properties to convert electronic energy into proton motive force, a fundamental step that might contribute to the proton electrochemical gradient across the bacterial cytoplasmic membrane [20]. The mechanism that allows PpcA to perform such concerted e^-/H^+ transfer is driven by the protonation/deprotonation of a redox-Bohr center, which was assigned to the heme IV propionate 13 (P^{IV}_{13}, according to the IUPAC nomenclature) [21]. The protonation/deprotonation of this center leads to conformational changes in residues located in its vicinity, which were mapped on the solution structure of PpcA [21]. Given the significance of the residue Phe^{15}, it was replaced by site-directed mutagenesis with a leucine in the triheme cytochrome PpcA (hereafter designated PpcAF15L) and the impact of the substitution on the redox properties of the protein was evaluated [19]. This study showed that replacing Phe^{15} with leucine disrupted the balance of the global network of cooperativities, preventing the mutant protein from performing the concerted electron/proton transfer which is crucial to the function of PpcA.

In order to rationalize these observations in structural terms, we have produced ^{15}N-labeled PpcAF15L and determined its solution structure. In addition, the solution structure was used to monitor the pH-dependent conformational changes. The comparison of the solution structures of PpcAF15L and PpcA reveals the structural features associated with conserved residue Phe^{15} and its role in the functional mechanism of PpcA.

2. Materials and methods

2.1. Site directed mutagenesis

For mutagenesis, QuikChange Site-Directed Mutagenesis Kit (Stratagene) was used in accordance with the manufacturer's instructions. Oligonucleotides were synthesized by MWG Biotech (High Point, NC). PpcA expression vector pCK32 [22] was used as a template. The presence of the F15L mutation was confirmed by DNA sequencing performed by MWG Biotech.

2.2. Bacterial growth and protein purification

Uniformly ^{15}N labeled and unlabeled PpcAF15L were expressed in *Escherichia coli* as previously described [19]. Briefly, PpcAF15L was expressed in plasmid pCK32 in *E. coli* BL21(DE3) by co-expression with plasmid pEC86 that encodes for the cytochrome *c* maturation gene cluster [23]. Cells were grown in 2xYT medium and, after reaching an OD_{600} of ~1.5, cultures were processed in either of two ways: (a) addition of 10 μM isopropyl β-D-thiogalactoside (IPTG) and growing overnight at 30 °C to express unlabeled protein, followed by harvesting by centrifugation; (b) cells were collected by centrifugation, washed twice with 250 mL M9 medium, resuspended in minimal media (in a ratio of 250 mL of minimal medium for each liter of 2xYT medium) supplied with 1 g/L $^{15}NH_4Cl$ as nitrogen source (together with 1 mM of the heme precursor α-aminolevulinic acid, trace amounts of metal ion salts, biotin and thiamine), grown overnight at 30 °C in the presence of 0.8 mM IPTG and harvested by centrifugation. Isolation of the periplasmic fraction and purification of the protein was done as previously described [19,24].

2.3. NMR sample preparation

PpcAF15L was lyophilized twice and then resuspended in 45 mM sodium phosphate buffer (100 mM ionic strength) pH 7.1 (measured using a glass microelectrode without correction for isotope effects). ^{15}N labeled and unlabeled samples were prepared to a final concentration of approximately 1 mM in 92% H_2O/8% ^2H_2O or in pure ^2H_2O. In order to avoid oxidation of the samples, the NMR tubes were sealed with a gas-tight serum cap and the air was flushed out from the sample. All the samples were then fully reduced with catalytic amounts of hydrogenase from *Desulfovibrio vulgaris* (Hildenborough) under a hydrogen atmosphere, as previously described [19].

2.4. NMR spectroscopy

All NMR spectra were recorded at 298 K and pH 7.1 on a Bruker Avance 600 MHz spectrometer equipped with triple-resonance cryoprobe. For the ^{15}N labeled sample, 2D-^1H–^{15}N heteronuclear single quantum coherence (HSQC) experiments were acquired. For the unlabeled sample, the following set of NMR experiments were acquired: 2D-^1H correlation spectroscopy (COSY), 2D-^1H total correlation spectroscopy (TOCSY) with 60 ms mixing-time, and 2D-^1H nuclear Overhauser effect spectroscopy (NOESY) with 50 ms mixing-time. 2D-^1H TOCSY (45 ms mixing-time) and 2D-^1H NOESY (100 ms mixing-time) NMR spectra were also acquired for the unlabeled sample prepared in pure ^2H_2O to assist in the assignment of the heme proton signals. Before and after all two dimensional experiments, 1D-^1H NMR spectra were recorded in order to verify the protein integrity and full reduction. ^1H and ^{15}N chemical shifts were calibrated using the water signal as internal reference and through indirect referencing, respectively [25]. TOPSPIN software (Bruker Biospin, Karlsruhe, Germany) was used to process all NMR spectra, which were then analyzed with Sparky (TD Goddard and DG Kneller, Sparky 3, University of California, San Francisco, USA).

A series of two dimensional ^1H–^{15}N HSQC spectra were acquired in the pH range 5.4 to 9.5 to monitor the effect of pH on the amide signals. To adjust the pH of the samples, minimal amounts of either NaO^2H or ^2HCl were added inside an anaerobic glove chamber at <1 ppm oxygen (MBraun LABstar) to avoid sample oxidation. The weighted average chemical shift ($\Delta\delta_{avg}$) of each backbone and side chain amide was calculated as: $\Delta\delta_{avg} = \sqrt{[(\Delta\delta^2N/25 + \Delta\delta^2H)/2]}$, where ΔδH and ΔδN are the differences in the ^1H and ^{15}N chemical shifts, respectively [26].

2.5. Assignment and determination of restraints

PpcAF15L assignments, including backbone, side chain and heme resonances, were made as previously described for the wild-type protein [27] and data was deposited in the BioMagResBank (http://www.bmrb.wisc.edu) under BMRB accession number 18787.

For structure determination, the cross-peaks assigned in the 50 ms 2D-^1H-NOESY spectra were integrated using the program Sparky. As described for the wild-type protein, the integration of the isolated cross-peaks of the PpcAF15L mutant was performed with a Gaussian function and for the overlapped cross-peaks the integration was performed with sum data in a box surrounding it. Volumes of cross-peaks were converted into volume restraints and used as input for the program PARADYANA [28]. Initial structures were calculated with a preliminary set of NOE data and the resulting conformers were then analyzed and used to assign additional peaks in the NOESY spectra. The program GLOMSA [29] was used for stereospecific assignment during the process of structure calculation. Three non-standard residues were used for structure calculations: fast-flipping aromatic residues with pseudo-atoms to limit the orientations of the planes, flexible heme groups and proline residues with fixed upper limit distances for ring closure. A set of 69 fixed upper limit distances associated with these residues was also used as input for PARADYANA. In the final stages of structure refinement, the calculated structures were checked for short (less than 2.5 Å) distances between assigned protons that should give rise to significant NOEs.

2.6. Structure calculation and analysis

As for the wild-type protein, the solution structure of PpcAF15L was calculated with the program PARADYANA. In each calculation,

200 conformers were determined and the 10 structures with lowest target function value were selected for further visual analyses using the program CHIMERA (version 1.5.1) [30]. In the final calculation, 20 structures with lowest target function values were selected. The program MOLMOL [31] was used to superimpose, identify elements of secondary structure in the final set of conformers, and also to compare the structures obtained for mutant and wild-type proteins. The quality of the structures was analyzed with PROCHECK-NMR [32]. The coordinates were deposited in the Protein Data Bank under accession code 2LZZ.

3. Results

3.1. Sequential assignment, restraints and structure calculation of PpcAF15L

With the exception of the first two residues, the NMR signals of all the other backbone, side chains and heme substituents were assigned following the same methodology used for the wild-type protein [21]. To avoid overlap with polypeptide amide protons, the heme signals were assigned in the NMR spectra acquired for PpcAF15L samples prepared in ^2H_2O, according to the strategy described by Turner and co-workers [33]. Following that, individual spin-systems were first identified in the NMR spectra acquired in H_2O, according to their type, and then specific assignments were made. A summary of the sequential connectivities between NH, Hα and Hβ protons is shown in Supplementary Fig. S1. The total extent of assignment for PpcAF15L is 88%, excluding carboxyl, amino and hydroxyl groups.

The assigned cross-peaks in the 2D-^{1}H NOESY spectrum were integrated and converted into volume restraints, resulting in 806 lovs (lower limits for volumes) and 1016 upvs (upper limits for volumes) (Table 1). These were used as input for the program PARADYANA [28] together with a set of 69 fixed upper limit distances. The preliminary structures were analyzed using the program GLOMSA [29], modified to take NOE volumes as input, and 34 stereo-specific assignments were made for diastereotopic pairs of protons or methyl groups. The effect of spin diffusion introduces an uncertainty into the conversion of experimental data into distance restraints. This effect was simulated by complete relaxation matrix calculations based on the initial protein structures and, accordingly, a parameter was set in the program PARADYANA to loosen all distance restraints by 5%. An average of 25 NOE restraints per residue (11 lovs and 14 upvs) and 122 per heme residue (54 lovs and 68 upvs) were used for the final calculation (Fig. 1). The distribution of the number of restraints is not uniform along the protein sequence, as heme groups attached to positions 30, 54 and 68 show many long-distance contacts, a feature in common with the wild-type protein [21].

Table 1
Summary of restraint violations and quality analysis for the final family of solution structures for PpcAF15L.

Parameter	
Type of distance restraint	
Intra-residue	704
Sequential	365
Medium range ($2 \leq \|i-j\| < 5$)	300
Long range ($\|i-j\| \geq 5$)	453
Total	1822 (806 lovs + 1016 upvs)
Upper distance limit violations	
Average maximum	0.26 ± 0.05
Number of consistent violations (>0.2 Å)	0
Lower distance limit violations	
Average maximum	0.27 ± 0.04
Number of consistent violations (>0.2 Å)	0
Van der Waals violations	
Average maximum	0.19 ± 0.02
Number of consistent violations (>0.2 Å)	0
Ramachandran plot (%)[a]	
Most favored regions	62.6
Additionally allowed regions	35.2
Generously allowed regions	2.2
Disallowed regions	0.0
Stereospecific assignments[b]	34
Precision	
Average pairwise rmsd backbone (Å)	0.36 ± 0.12
Average pairwise rmsd heavy atoms (Å)	1.14 ± 0.10

[a] Values obtained with PROCHECK-NMR.
[b] Analysis with GLOMSA.

3.2. Quality analysis of the structures

The final family consists of 20 structures (Fig. 2A) with the lowest target function values (from 2.36 to 2.65 Å^2 with an average value 2.56 Å^2, 12% range from the lowest value). The structures superimpose with an average pairwise backbone (N–Cα–C′) rmsd of 0.36 Å and a heavy atom rmsd of 1.14 Å (Supplementary Fig. S2). Thus, the backbone is well defined and the amino acid side chains show larger conformational variability in regions with higher solvent exposure. In particular, the N- and the C-termini are disordered. The statistics for this family of structures are shown in Table 1. The Ramachandran plot shows 62.6% of the residues are in the most favored regions, 37.4% in the allowed regions. A total of 46 hydrogen bonds were identified in the family of 20 structures with the program MOLMOL [31], 23 of which were present in at least 50% of the structures.

3.3. pH titration

The pH titration of PpcAF15L was monitored by ^{1}H–^{15}N HSQC NMR in the pH range 5.4–9.5 and all ^{1}H and ^{15}N chemical shifts of the polypeptide backbone (except for residues 1 and 2) and side chains were measured. To estimate the effects of pH change on the PpcAF15L solution structure, the average chemical shift differences of each amide signal ($\Delta\delta_{avg}$) were calculated as described by Garret and co-workers [26]. The residues whose NH signals showed larger differences were from Lys^7, Ala^8, Asn^{10}, Ile^{38} backbone, and also from Asn^{10} and Gln^{21} side chains (Fig. 3A). The pH titrations of these signals are shown in Fig. 3B. The NH signals of Lys^7, Ala^8, Asn^{10} and Gln^{21} have basic pK_a values of 7.6, 7.7, 7.6 and 8.2 respectively, whereas Ile^{38} has a much more acidic pK_a (5.2).

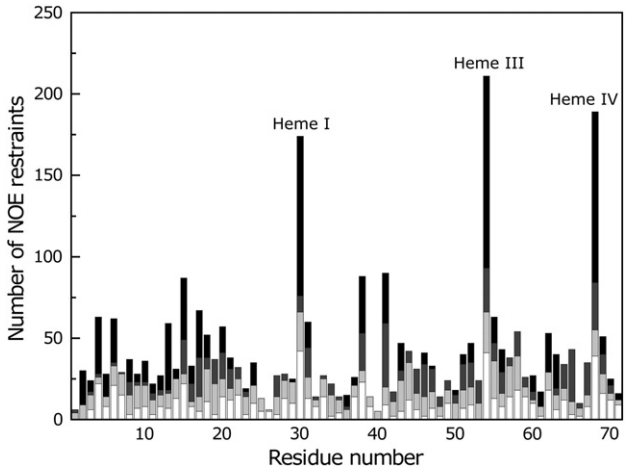

Fig. 1. Number of restraints per residue used for the calculation of the structure of PpcAF15L. Bars are white, light gray, dark gray and black for intraresidue, sequential, medium and long range restraints, respectively. Residues 30, 54 and 68 also include restraints to hemes I, III and IV, respectively.

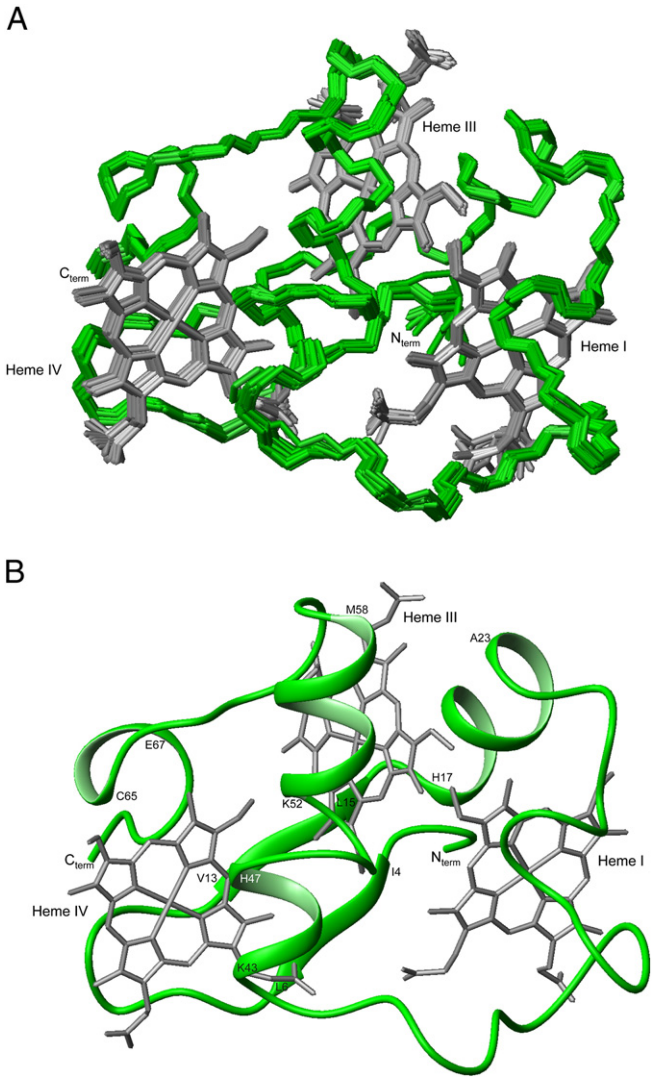

Fig. 2. PpcAF15L solution structure. (A) Overlay of the 20 lowest energy NMR solution structures of PpcAF15L at pH 7.1. Superimposition was performed using all the heavy-atoms. The peptide chain and the hemes are colored green and gray, respectively. (B) Ribbon diagram of PpcAF15L structure. Figures were produced using MOLMOL [31].

4. Discussion

The comparable dispersion of the amide signals in the $^{1}H–^{15}N$ HSQC NMR spectra obtained for PpcAF15L and wild-type proteins indicates that the overall native fold is maintained in the mutant (Fig. 4). However, several signals are significantly affected, namely the backbone NH signals of Ile[4], Val[5] and the segment formed by residues His[17]-Val[24] (see inset in Fig. 4). The amide signal of His[17] is shifted the most, followed by that of His[20]. The backbone NH signals of residues Asp[26]-Lys[28], Gly[36]-Lys[37], Ala[46] and Gly[53] are affected to smaller extent. The polypeptide sequence of both proteins contains one asparagine (Asn[10]), one glutamine (Gln[21]) and six axial histidines (His[17(I)], His[20(III)], His[31(I)], His[47(IV)], His[55(III)] and His[69(IV)]), which have an additional amide or amine group in their side chains. Inspection of these signals in the $^{1}H–^{15}N$ HSQC NMR spectra showed that the amide signals of Gln[21] and heme III axial histidine (His[20(III)]) are the most affected, followed by those of His[47(IV)] and His[55(III)]. Comparison of the heme proton chemical shifts was previously reported and showed that the largest difference was for the thioether proton $3^{2}CH_{3}^{III}$, due to the additional ring-current effects from Phe[15] aromatic ring in the native protein, which is not present in PpcAF15L [19].

The number of residues per heme group in PpcAF15L is approximately 23 and, consequently, several nuclei are located in close proximity of the hemes. Since the heme groups are diamagnetic in the reduced state, the observed chemical shifts of those signals might have large contribution from the heme(s) ring-current effects. Consequently, some signals might show significant changes in their chemical shifts even in presence of marginal structural rearrangements. Therefore, to properly rationalize the changes observed in the redox properties and concomitant functional mechanism of PpcAF15L, it is essential to determine the solution structure of this mutant.

4.1. Comparison of PpcAF15L and PpcA solution structures

The comparison between the lowest-energy NMR structures of PpcAF15L and PpcA showed a rmsd of 1.08 Å for backbone atoms (Fig. 5). The global fold of the wild-type is maintained in the mutant protein, though local rearrangements of polypeptide chain were observed (Fig. 4). The solution structure of PpcAF15L folds in a two-strand antiparallel β-sheet at the N-terminus formed by Ile[4]-Leu[6] and Val[13]-Leu[15], followed by three α-helices between residues His[17]-Ala[23], Lys[43]-His[47] and Lys[52]-Met[58] and a 3_{10}-helix segment formed between residues Cys[65]-Glu[67] (Fig. 2B). In PpcA residues Ile[4] and Val[5] are located opposite to Phe[15] in the two-stranded antiparallel β-sheet [21]. These residues are clearly perturbed in the mutant. Another region showing important structural rearrangements is the first α-helix, located between hemes I and III. This helix is formed by residues His[17]-Ala[23] in the mutant, whereas in the wild-type it comprises residues Ala[19]-Lys[22]. Finally, a 3_{10}-helical segment is formed between residues Cys[65]-Glu[67] only in the mutant.

The parameters describing the heme geometry of PpcAF15L in solution are presented in Table 2. The geometry of the heme core is essentially conserved in comparison with the wild-type (Table 2). The iron–iron distances differ by less than 0.03%. Hemes I and IV are nearly parallel to each other, though slightly more so in the mutant and nearly perpendicular to heme III. However, the heme axial ligand geometry is different for all the three hemes (see Table 2 and Fig. 6), highlighting the important structural role played by the conserved residue Phe[15] in determining the geometry of the axial heme ligands in the wild-type protein.

4.2. Heme reduction potentials and redox interactions

The characterization of the redox properties of PpcAF15L and PpcA was previously reported in detail and is summarized in Table 3 [19]. The solution structure determined in the present work allows the structural basis for the differences observed in the redox properties of PpcAF15L and PpcA to be addressed. The heme reduction potentials in the mutant are also modulated by heme–heme redox interactions, as for the wild-type. The positive values obtained for the redox interactions suggest that they are dominated by electrostatic effects (Table 3). The highest and the lowest redox interaction (36 and 14 mV, respectively) are observed between the closest (III–IV) and farthest (I–IV) pairs of heme groups. The similarity of the redox interaction values in the two proteins correlates with the conserved heme iron–iron distances (Table 2) and with the similar distribution of charged residues in the proteins.

The reduction potentials in the mutant are also negative, as expected for relatively exposed *c*-type hemes with bis-histidine axial coordination. In the lowest energy structure, the heme exposures are 253.2 Å^2 (231.7 Å^2 for PpcA), 168.1 Å^2 (215.8 Å^2) and 207.8 Å^2 (171.3 Å^2) for hemes I, III and IV respectively. The slightly higher solvent exposure of hemes I and IV in the mutant correlates with their more negative reduction potential values when compared with the wild-type. The potential of heme IV is the least negative in both mutant and wild-type, and can also be rationalized by its location in a substantially positive environment due to the presence of

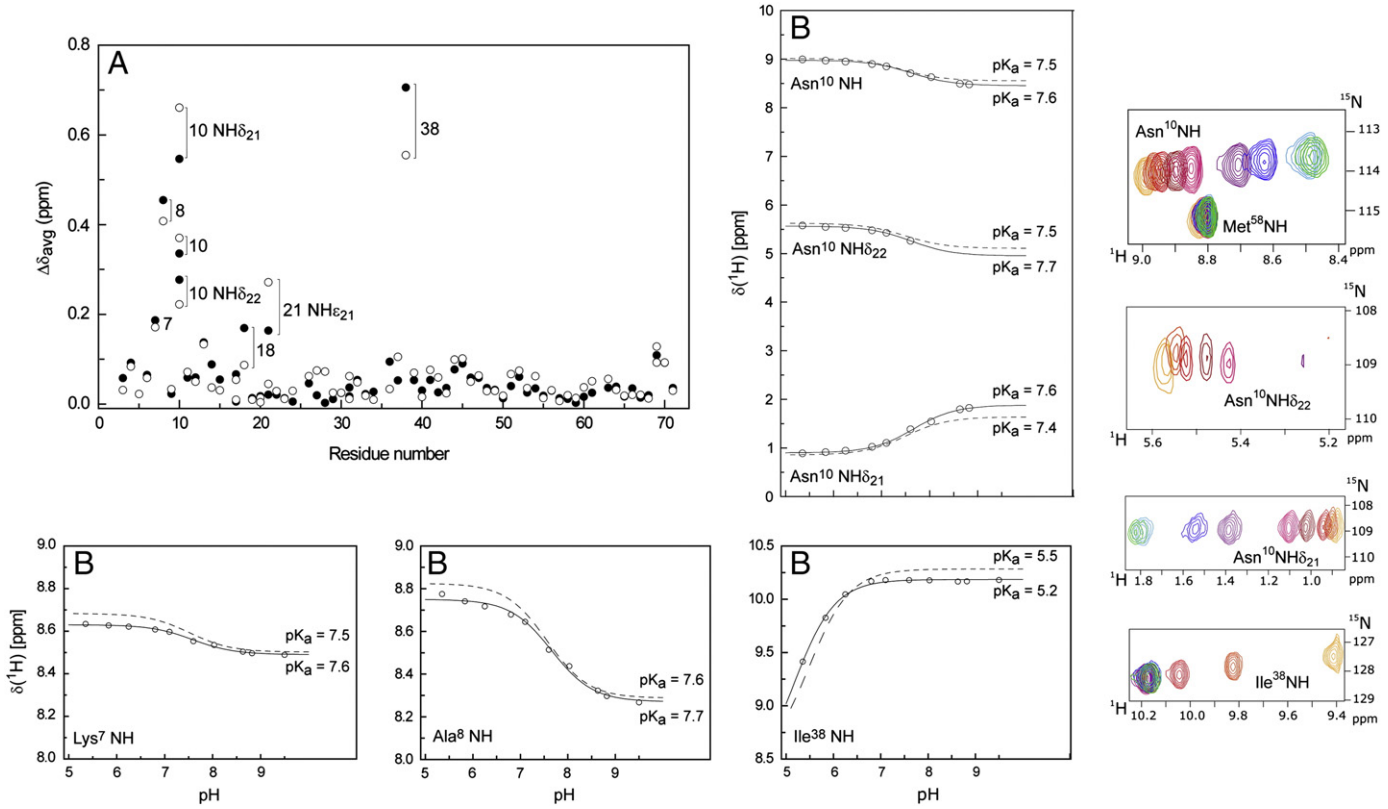

Fig. 3. Comparison of pH-linked conformational changes in PpcAF15L (open circles) and PpcA (closed circles). (A) Weighted average of ^{1}H and ^{15}N chemical shifts ($\Delta\delta_{avg}$) between pH 5.4 and 9.5. (B) pH titration data of the most affected PpcAF15L amide signals. The dashed lines in each panel represent the best fit for the wild-type protein. In the expansion of each ^{1}H–^{15}N-HSQC NMR spectrum, pH increases from yellow to green. Lys^{7} and Ala^{8} backbone amide signals are not shown since they appear in a very crowded region of the spectra.

several neighboring lysine residues that stabilize its reduced state. Additionally, the angles between the axial histidine ring planes vary by approximately 30° (Table 2 and Fig. 6), which are also expected to contribute to the modulation of heme reduction potentials. Detailed structural and electrochemical studies performed in cytochrome b_5 by Sarma and co-workers [34,35] showed that the orientation of

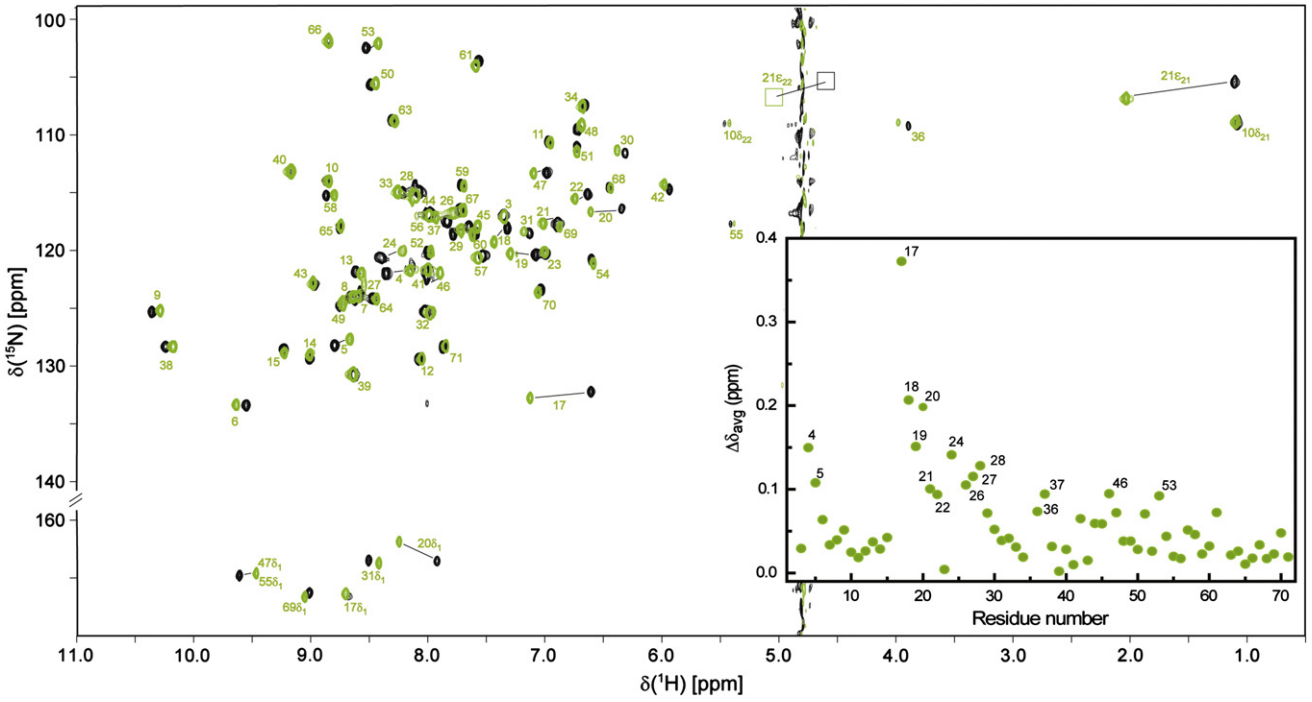

Fig. 4. 2D-^{1}H–^{15}N HSQC NMR spectra of fully reduced PpcAF15L (green contours) and PpcA (black contours). The most affected signals are connected by a straight line in the spectrum. In the inset the weighted average of ^{1}H and ^{15}N chemical shifts ($\Delta\delta_{avg}$) of each backbone amide is represented. The squares indicate the εNH_2 position of residues Gln^{21}, which have small intensity due to their close proximity to the water signal and are not visible at the spectra level represented in the figure.

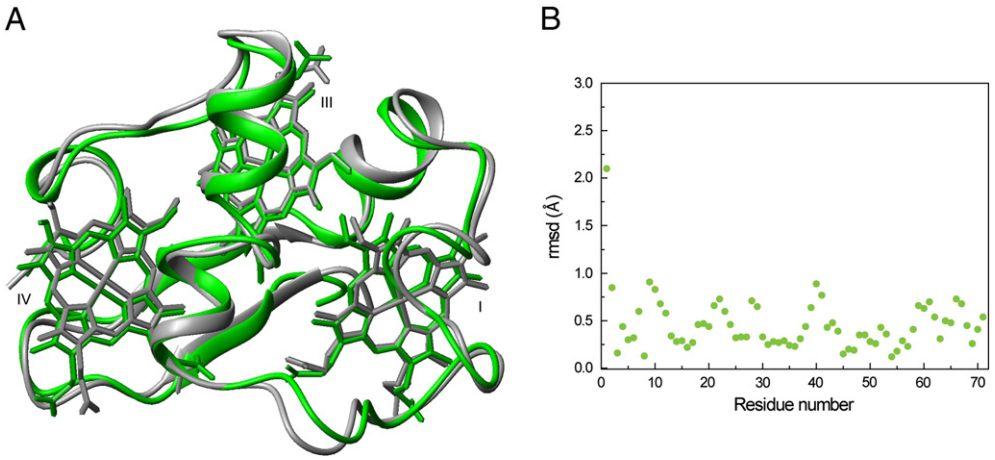

Fig. 5. Comparison of PpcAF15L and PpcA lowest energy solution structures. Structures were superimposed in MOLMOL [31] using backbone atoms. (A) PpcAF15L *versus* PpcA solution structure (PDB ID: 2LDO [31]). PpcAF15L and PpcA solution structures are colored green and gray, respectively. (B) Average rmsd between each pair of residues.

axial ligand ring planes slightly modulates the reduction potentials of bis-(imidazole) axially ligated heme proteins.

The reduction potential of heme III is the most affected in the mutant (Table 3). The change in the reduction potential of heme III cannot be rationalized by the heme solvent exposure or by the small changes observed in the geometry of the axial ligands alone. A significant factor could be the structural rearrangements in the first α-helix. This helix is longer in the mutant (His^{17}-Ala^{23} *versus* Ala^{19}-Lys^{22}) compared to the wild-type. It covers one side of heme III and contains two positively charged residues, Lys^{18} and Lys^{22}. Their proximity to heme III is likely to affect its reduction potential by reorientation towards the solvent. However, the ends of both the lysine side chains are disordered in both proteins, preventing a detailed analysis of their electrostatic effects. Considerable variations in the chemical shifts of the signals of $His^{17(I)}$, $His^{20(III)}$ and Gln^{21} are also observed (Fig. 4). In PpcA, the side chains of $His^{17(I)}$ and $His^{20(III)}$, together with the aromatic ring of residue Phe^{15}, are part of the protein hydrophobic core in the proximity of heme III (Fig. 7A). The superposition of the mutant and wild-type solution structures shows that the side chains of Leu^{15} and Phe^{15} occupy equivalent positions (Fig. 7B). Thus, the replacement of the aromatic ring by the aliphatic side chain removes the aromatic–aromatic interaction between Phe^{15} and heme III and thereby influences the heme redox properties. Furthermore, the aromatic ring of Phe^{41} at the bottom of the cleft below heme III (Fig. 7C) is rotated by approximately 30°, which could give rise to different ring stacking effects contributing to the change in heme III redox properties. Overall, these important structural rearrangements in the hydrophobic region in the vicinity of heme III alter the nature of the heme-aromatic interactions affecting the reduction potential of heme III.

Cytochromes c_3 isolated from *Desulfovibrio* spp. are also periplasmic proteins which play a central role in energy transduction by coupling the transfer of electrons and protons from hydrogenase. By receiving both electrons and protons that result from the conversion of H_2, the redox-Bohr effect in cytochromes c_3 allows part of the free energy of the conversion to be used to release protons in the more acidic environment of the periplasm [36,37]. The structural motif formed by F15 and hemes I and III is also conserved in the tetraheme cytochrome c_3 family, in which F20 occupies an equivalent position. There are biochemical studies reported for F20 mutants of *D. vulgaris* tetraheme cytochromes c_3 isolated from the strains Hildenborough ($DvHc_3$) and Miyazaki ($DvMc_3$) [38–40]. In the case of $DvHc_3$, in which F20 was also replaced by leucine, it was shown that the macroscopic redox potentials were globally affected [38]. Moreover, it was proposed by the authors that the intramolecular electron exchange between heme III and heme I was drastically affected by the F20L replacement [38]. In the highly homologous tetraheme cytochrome $DvMc_3$, the roles of aromatic residues in

Table 2
Heme geometry for PpcAF15L (this work) and PpcA [20] cytochromes in solution. The values for both proteins were obtained for the lowest-energy structure.

	PpcA	PpcAF15L
Heme Fe–Fe distance (Å)		
I–III	11.7	11.4
I–IV	19.0	18.9
III–IV	12.6	12.7
Angle between heme planes (°)		
I–III	82	78
I–IV	27	12
III–IV	74	71
Angle between His planes (°)		
I	50	80
III	23	50
IV	80	52

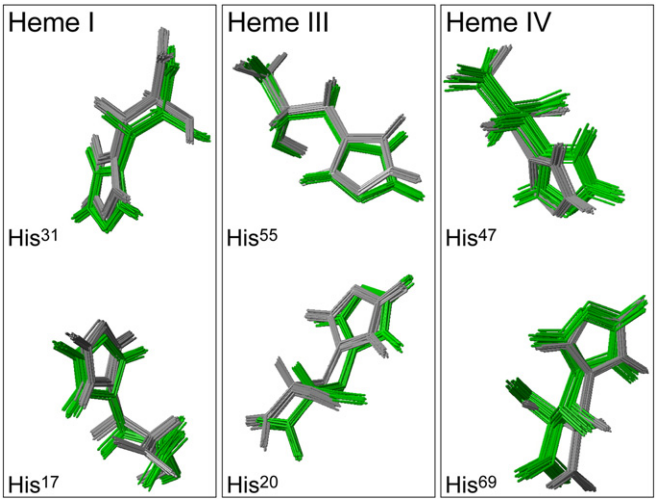

Fig. 6. Orientation of the axial histidines of each heme group for PpcAF15L (green) and PpcA (gray) solution structures. Structures were superimposed in MOLMOL [31] using backbone atoms. The axial histidine orientations taken from all the 20 structures are presented to show the geometry consensus among the entire family of structures.

Table 3
Heme reduction potentials and pairwise interactions (mV) of the fully reduced and protonated forms of PpcAF15L [21] and PpcA [19]. The standard errors are given in parentheses.

	Heme redox potentials			Redox interactions			Redox-Bohr interactions		
	I	III	IV	I–III	I–IV	III–IV	I–H	III–H	IV–H
PpcAF15L	−164(4)	−168(4)	−136(5)	24(2)	14(2)	36(2)	−20(4)	−17(4)	−49(4)
PpcA	−154(5)	−138(5)	−125(5)	27(2)	16(3)	41(3)	−32(4)	−31(4)	−58(4)

redox regulation of hemes were also investigated by site-directed mutagenesis of every aromatic residue except for the axial ligands [40]. This study showed that the mutations of F20 had large chemical shift changes in the NMR signals for hemes I and III, and large changes in the reduction potentials of hemes I and III. Unfortunately, there has been no description of detailed microscopic thermodynamic properties for these two cytochromes and, consequently, the effect of replacing the conserved F20 residue and its effects on heme III potential in cytochromes c_3 cannot be evaluated further. Nonetheless, the macroscopic data obtained for DvHc_3 and DvMc_3, together with the detailed structural and functional properties obtained for PpcA and PpcAF15L, provide a rationale for the conserved structural motif formed by F15 (F20 in the tetraheme cytochrome c_3 family) and hemes I and III.

4.3. Structural mapping of the redox-Bohr center

The heme reduction potentials are modulated by the solution pH as well as by redox interactions (Table 3). This modulation, known as the redox-Bohr effect, is crucial for the function of PpcA, which can couple electron and proton transfer at physiological pH [19]. The detailed thermodynamic characterization of PpcA showed that such coupling involved the microstates P_{1H} (protonated microstate with heme I oxidized) and P_{14} (deprotonated microstate with hemes I and IV oxidized) [20]. Thus, part of the energy associated with electrons received from the donor by microstate P_{1H} is used by the protein to lower the pK_a value of the redox-Bohr center so that protons can be released in the periplasm at physiological pH. This mechanism implies conformational changes in the neighborhood of the redox-Bohr center, which was assigned to heme IV propionate 13 (P^{IV}_{13}) in the wild-type protein [21]. The proposed mechanism involved disruption of a hydrogen bond between the O7 of P^{IV}_{13} and the carbonyl oxygen of Lys^7, located at the β-turn, causing the observed pH-linked conformational changes of residues Lys^7, Ala^8 and Asn^{10} [21].

The properties of the PpcAF15L redox-Bohr center are different (Table 3). However, as in the wild-type, the redox-Bohr interaction for heme IV is considerably higher than for the others, suggesting that the redox-Bohr center is also located in the vicinity of heme IV. The analysis of the chemical shift variation of the NH signals in the pH range 5.4–9.5 showed that the same set of signals (backbone NH of Lys^7, Ala^8, Asn^{10}, Ile^{38} and the side chains of Asn^{10} and Gln^{21}) is the most affected in both proteins, but to different extents (*cf.* open and closed symbols in Fig. 3A and solid and dashed lines in Fig. 3B).

The residues Lys^7, Ala^8 and Asn^{10} are part of the β-turn connecting the two-strand β-sheet near heme IV; Gln^{21} is located in the first α-helix between I and III, whereas Ile^{38} is a fully conserved residue within the family of *G. sulfurreducens* triheme cytochromes c_7 and forms a conserved hydrogen bond between the backbone amide proton and the carboxyl oxygen of P^{I}_{13} [41]. The pK_a of the backbone NH of residue Ile^{38} is more acidic (pK_a 5.2 *versus* an average value of 7.8 for the other NH groups) and the decrease of the proton chemical shift at low pH correlates with the disruption of a hydrogen bond between the amide proton and the carboxyl oxygen of P^{I}_{13} upon protonation of the latter. Similar behavior was observed in the wild type, but the smaller $\Delta\delta_{avg}$ value (0.56 *versus* 0.71 ppm in the wild-type) and the lower pK_a (5.2 *versus* 5.5 in the wild-type) are indicative of structural rearrangements of the mutant protein in this region.

The chemical shifts of Gln^{21} side chain amide protons (εNH_2) are strongly shifted upfield (2.04 and 5.08 ppm) compared to their average position at 7.1 ppm, obtained from approximately 10^4 chemical shifts as reported in the Biological Magnetic Resonance Data Bank (http://www.bmrb.wisc.edu/ref_info/statsel.htm#4). This feature was already noted for the wild type in which the εNH_2 protons of Gln^{21} were observed at 1.11 and 4.56 ppm [27]. These protons are located in close proximity to His$^{17(I)}$ ring (Fig. 8) and, thus, are subject to

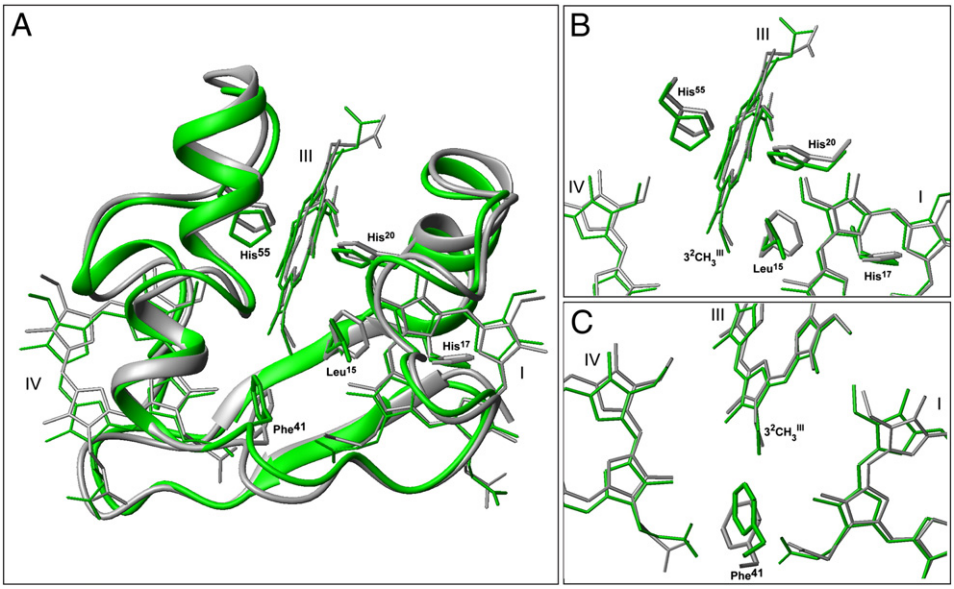

Fig. 7. Comparison of PpcAF15L (green) and PpcA (gray) lowest energy solution structures. Structures were superimposed in MOLMOL [31] using backbone atoms. (A) General overview of the heme core, (B) heme core region containing the side chains of residues Phe^{15}, His$^{17(I)}$ and His$^{20(III)}$, (C) heme core region containing side chain of residue Phe^{41}.

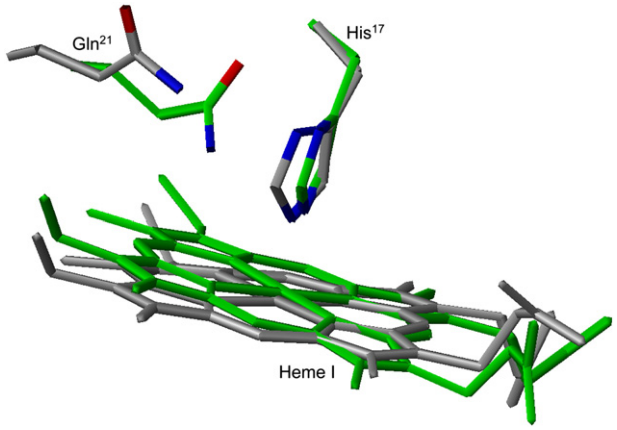

Fig. 8. Spatial disposition of residues Gln[21] and His[17], which are located in the close proximity of heme I, in PpcAF15L (green) and PpcA (gray) solution structures. Structures were superimposed in MOLMOL [31] using backbone atoms.

additional local magnetic fields originating from heme I ring-currents; the nearly axial position in relation to heme I explains their upfield shift. The residue Gln[21] is located far from the redox-Bohr center (see below) and the pH dependence of the εNH_2 protons is probably due to protonation of groups in vicinity of the glutamine residue, with the side chain of Lys[18] as a likely candidate as its NH signal also shows a considerable chemical shift variation.

On the other hand, the pK_a values obtained for the NH signals of Lys[7], Ala[8] and Asn[10] correlate with the pK_a of the redox-Bohr centers (8.5 *versus* 8.6 in the wild-type) previously determined for the fully reduced and protonated protein [19]. Thus, as in the wild-type, the pH dependence is likely to be caused by the protonation/deprotonation of the redox-Bohr group, which can also be assigned to P_{13}^{IV} in the mutant. This propionate group is considerably less exposed to solvent than P_{17}^{IV} in both proteins (the accessible surface area of the P_{13}^{IV} and P_{17}^{IV} propionate oxygens for PpcA are 16.3 Å^2 and 44.1 Å^2, respectively and those for F15L mutant are 12.9 Å^2 and 40.7 Å^2). Therefore, it is not surprising that the pK_a of the chemical shifts of NH groups of residues Lys[7], Ala[8], Asn[10], located in the vicinity of P_{13}^{IV}, showed similar behavior upon protonation/deprotonation of the redox-Bohr center. However, these signals showed different $\Delta\delta_{avg}$ values, which can be explained by the conformational rearrangements observed in vicinity of heme IV (Fig. 9). These rearrangements include the slight reorientation of heme IV in relation to heme I (Table 2) and also the positioning of the β-turn between the antiparallel two-strand β-sheet that contains residues Lys[7], Ala[8] and Asn[10]. Altogether, the local rearrangements observed in the neighborhood of the redox-Bohr center are likely the cause of the different redox-Bohr interactions in the two proteins.

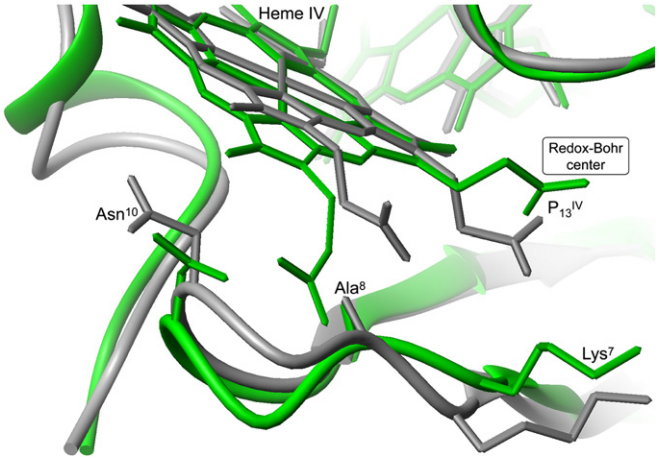

Fig. 9. Structural map of residues involved in the pH-dependent conformational changes in vicinity of redox-Bohr center P_{13}^{IV} in PpcAF15L (green) and PpcA (gray) solution structures. Structures were superimposed in MOLMOL [31] using backbone atoms.

5. Conclusions

The structure of PpcAF15L mutant determined in the present work sheds light on the role of the strictly conserved amino acid Phe[15] in fine-tuning the heme reduction potentials and the network of redox and redox-Bohr cooperativities that are crucial for the functional mechanism of PpcA. Though the overall folding of the protein was not affected, important local structural rearrangements caused by the replacement of Phe[15] by a leucine residue were observed. These structural rearrangements had an effect in lowering the reduction potentials of the hemes and altered the properties of the redox-Bohr center. The analysis of the chemical shift variation of the backbone and side chain amide signals with pH allowed mapping of the pH-linked conformational changes caused by protonation/deprotonation of the redox-Bohr center, which was assigned to heme propionate P_{13}^{IV}. These changes unbalance the redox networks observed in the wild-type protein and alter the distribution of the protein microstates during its redox cycle. As a consequence, while a concerted e^-/H^+ transfer gives the wild-type protein the necessary thermodynamic properties to convert electronic energy into proton motive force, a fundamental step that might contribute to the proton electrochemical gradient across the bacterial cytoplasmic membrane, in the mutant this feature is no longer observed, highlighting the important role played by the residue Phe[15] in the functional mechanism of PpcA.

Acknowledgements

This work was supported by the Fundação para a Ciência e a Tecnologia (Portugal) grants PTDC/QUI/70182/2006 and PEst-C/EQB/LA006/2011. J.M.D. and L.M. are recipient of a BI and BPD under the scope of the project PTDC/QUI/70182/2006, respectively. We acknowledge LabRMN at FCT-UNL and Rede Nacional de RMN for access to the facilities. Rede Nacional de RMN is supported with funds from FCT, Projecto de Re-equipamento Científico, Portugal (project number REDE/1517/RMN/2005). P.R.P. is supported by the division of Chemical Sciences, Geosciences, and Biosciences, Office of Basic Energy Sciences of the U.S. Department of Energy program under contract no. DE-AC02-06CH11357.

Appendix A. Supplementary data

Supplementary data to this article can be found online at http://dx.doi.org/10.1016/j.bbabio.2012.12.008.

References

[1] B.C. Kim, B.L. Postier, R.J. Didonato, S.K. Chaudhuri, K.P. Nevin, D.R. Lovley, Insights into genes involved in electricity generation in *Geobacter sulfurreducens via* whole genome microarray analysis of the OmcF-deficient mutant, Bioelectrochemistry 73 (2008) 70–75.
[2] H. Yi, K.P. Nevin, B.C. Kim, A.E. Franks, A. Klimes, L.M. Tender, D.R. Lovley, Selection of a variant of *Geobacter sulfurreducens* with enhanced capacity for current production in microbial fuel cells, Biosens. Bioelectron. 24 (2009) 3498–3503.
[3] H. Richter, K. McCarthy, K.P. Nevin, J.P. Johnson, V.M. Rotello, D.R. Lovley, Electricity generation by *Geobacter sulfurreducens* attached to gold electrodes, Langmuir 24 (2008) 4376–4379.
[4] M. Izallalen, R. Mahadevan, A. Burgard, B. Postier, R. Didonato Jr., J. Sun, C.H. Schilling, D.R. Lovley, *Geobacter sulfurreducens* strain engineered for increased rates of respiration, Metab. Eng. 10 (2008) 267–275.
[5] D.R. Bond, D.R. Lovley, Electricity production by *Geobacter sulfurreducens* attached to electrodes, Appl. Environ. Microbiol. 69 (2003) 1548–1555.
[6] J.E. Butler, N.D. Young, D.R. Lovley, Evolution of electron transfer out of the cell: comparative genomics of six *Geobacter* genomes, BMC Genomics 11 (2010) 40.
[7] D.R. Bond, D.E. Holmes, L.M. Tender, D.R. Lovley, Electrode-reducing microorganisms that harvest energy from marine sediments, Science 295 (2002) 483–485.
[8] D.R. Lovley, Bug juice: harvesting electricity with microorganisms, Nat. Rev. Microbiol. 4 (2006) 497–508.

[9] L.M. Tender, C.E. Reimers, H.A. Stecher III, D.E. Holmes, D.R. Bond, D.A. Lowy, K. Pilobello, S.J. Fertig, D.R. Lovley, Harnessing microbially generated power on the seafloor, Nat. Biotechnol. 20 (2002) 821–825.
[10] J.R. Lloyd, C. Leang, A.L. Hodges Myerson, M.V. Copi, S. Cuifo, B. Methe, S.J. Sandler, D.R. Lovley, Biochemical and genetic characterization of PpcA, a periplasmic *c*-type cytochrome in *Geobacter sulfurreducens*, Biochem. J. 369 (2003) 153–161.
[11] E.S. Shelobolina, M.V. Coppi, A.A. Korenevsky, L.N. Didonato, S.A. Sullivan, H. Konishi, H. Xu, C. Leang, J.E. Butler, B.C. Kim, D.R. Lovley, Importance of *c*-type cytochromes for U(VI) reduction by *Geobacter sulfurreducens*, BMC Microbiol. 7 (2007) 16.
[12] C. Leang, M.V. Coppi, D.R. Lovley, OmcB, a *c*-type polyheme cytochrome, involved in Fe(III) reduction in *Geobacter sulfurreducens*, J. Bacteriol. 185 (2003) 2096–2103.
[13] T.S. Magnuson, N. Isoyama, A.L. Hodges-Myerson, G. Davidson, M.J. Maroney, G.G. Geesey, D.R. Lovley, Isolation, characterization and gene sequence analysis of a membrane-associated 89 kDa Fe(III) reducing cytochrome *c* from *Geobacter sulfurreducens*, Biochem. J. 359 (2001) 147–152.
[14] J.E. Butler, F. Kaufmann, M.V. Coppi, C. Nunez, D.R. Lovley, MacA, a diheme *c*-type cytochrome involved in Fe(III) reduction by *Geobacter sulfurreducens*, J. Bacteriol. 186 (2004) 4042–4045.
[15] B.C. Kim, C. Leang, Y.H. Ding, R.H. Glaven, M.V. Coppi, D.R. Lovley, OmcF, a putative *c*-type monoheme outer membrane cytochrome required for the expression of other outer membrane cytochromes in *Geobacter sulfurreducens*, J. Bacteriol. 187 (2005) 4505–4513.
[16] T. Mehta, M.V. Coppi, S.E. Childers, D.R. Lovley, Outer membrane *c*-type cytochromes required for Fe(III) and Mn(IV) oxide reduction in *Geobacter sulfurreducens*, Appl. Environ. Microbiol. 71 (2005) 8634–8641.
[17] E. Afkar, G. Reguera, M. Schiffer, D.R. Lovley, A novel Geobacteraceae-specific outer membrane protein J (OmpJ) is essential for electron transport to Fe(III) and Mn(IV) oxides in *Geobacter sulfurreducens*, BMC Microbiol. 5 (2005) 41.
[18] D.R. Lovley, The microbe electric: conversion of organic matter to electricity, Curr. Opin. Biotechnol. 19 (2008) 564–571.
[19] J.M. Dantas, L. Morgado, Y.Y. Londer, A.P. Fernandes, R.O. Louro, P.R. Pokkuluri, M. Schiffer, C.A. Salgueiro, Pivotal role of the strictly conserved aromatic residue F15 in the cytochrome c_7 family, J. Biol. Inorg. Chem. 17 (2012) 11–24.
[20] L. Morgado, M. Bruix, M. Pessanha, Y.Y. Londer, C.A. Salgueiro, Thermodynamic characterization of a triheme cytochrome family from *Geobacter sulfurreducens* reveals mechanistic and functional diversity, Biophys. J. 99 (2010) 293–301.
[21] L. Morgado, V.B. Paixão, M. Schiffer, P.R. Pokkuluri, M. Bruix, C.A. Salgueiro, Revealing the structural origin of the redox-Bohr effect: the first solution structure of a cytochrome from *Geobacter sulfurreducens*, Biochem. J. 441 (2012) 179–187.
[22] Y.Y. Londer, P.R. Pokkuluri, D.M. Tiede, M. Schiffer, Production and preliminary characterization of a recombinant triheme cytochrome c_7 from *Geobacter sulfurreducens* in *Escherichia coli*, Biochim. Biophys. Acta 1554 (2002) 202–211.
[23] E. Arslan, H. Schulz, R. Zufferey, P. Kunzler, L. Thöny-Meyer, Overproduction of the *Bradyrhizobium japonicum c*-type cytochrome subunits of the cbb_3 oxidase in *Escherichia coli*, Biochem. Biophys. Res. Commun. 251 (1998) 744–747.
[24] A.P. Fernandes, I. Couto, L. Morgado, Y.Y. Londer, C.A. Salgueiro, Isotopic labeling of *c*-type multiheme cytochromes overexpressed in *E. coli*, Protein Expr. Purif. 59 (2008) 182–188.
[25] D.S. Wishart, C.G. Bigam, J. Yao, F. Abildgaard, H.J. Dyson, E. Oldfield, J.L. Markley, B.D. Sykes, ^{1}H, ^{13}C and ^{15}N chemical shift referencing in biomolecular NMR, J. Biomol. NMR 6 (1995) 135–140.
[26] D.S. Garrett, Y.J. Seok, A. Peterkofsky, G.M. Clore, A.M. Gronenborn, Identification by NMR of the binding surface for the histidine-containing phosphocarrier protein HPr on the N-terminal domain of enzyme I of the *Escherichia coli* phosphotransferase system, Biochemistry 36 (1997) 4393–4398.
[27] L. Morgado, V.B. Paixão, C.A. Salgueiro, M. Bruix, Backbone, side chain and heme resonance assignments of the triheme cytochrome PpcA from *Geobacter sulfurreducens*, Biomol. NMR Assign. 5 (2011) 113–116.
[28] D.L. Turner, L. Brennan, S.G. Chamberlin, R.O. Louro, A.V. Xavier, Determination of solution structures of paramagnetic proteins by NMR, Eur. Biophys. J. 27 (1998) 367–375.
[29] P. Güntert, W. Braun, K. Wüthrich, Efficient computation of three-dimensional protein structures in solution from nuclear magnetic resonance data using the program DIANA and the supporting programs CALIBA, HABAS and GLOMSA, J. Mol. Biol. 217 (1991) 517–530.
[30] E.F. Pettersen, T.D. Goddard, C.C. Huang, G.S. Couch, D.M. Greenblatt, E.C. Meng, T.E. Ferrin, UCSF Chimera — a visualization system for exploratory research and analysis, J. Comput. Chem. 25 (2004) 1605–1612.
[31] R. Koradi, M. Billeter, K. Wüthrich, MOLMOL: a program for display and analysis of macromolecular structures, J. Mol. Graph. 14 (1996) 51–55, (29-32).
[32] R.A. Laskowski, J.A. Rullmannn, M.W. MacArthur, R. Kaptein, J.M. Thornton, AQUA and PROCHECK-NMR: programs for checking the quality of protein structures solved by NMR, J. Biomol. NMR 8 (1996) 477–486.
[33] D.L. Turner, C.A. Salgueiro, J. LeGall, A.V. Xavier, Structural studies of *Desulfovibrio vulgaris* ferrocytochrome c_3 by two-dimensional NMR, Eur. J. Biochem. 210 (1992) 931–936.
[34] S. Sarma, R.J. DiGate, D.B. Goodin, C.J. Miller, R.D. Guiles, Effect of axial ligand plane reorientation on electronic and electrochemical properties observed in the A67V mutant of rat cytochrome b_5, Biochemistry 36 (1997) 5658–5668.
[35] S. Sarma, B. Dangi, C. Yan, R.J. DiGate, D.L. Banville, R.D. Guiles, Characterization of a site-directed mutant of cytochrome b_5 designed to alter axial imidazole ligand plane orientation, Biochemistry 36 (1997) 5645–5657.
[36] R.O. Louro, T. Catarino, J. LeGall, A.V. Xavier, Redox-Bohr effect in electron/proton energy transduction: cytochrome c_3 coupled to hydrogenase works as a 'proton thruster' in *Desulfovibrio vulgaris*, J. Biol. Inorg. Chem. 2 (1997) 488–491.
[37] J.M. Odom, H.D. Peck, Hydrogen cycling as a general mechanism for energy coupling in the sulfate-reducing bacteria, *Desulfovibrio* sp. FEMS Microbiol. Lett. 12 (1981) 47–50.
[38] A. Dolla, P. Arnoux, I. Protasevich, V. Lobachov, M. Brugna, M.T. Giudici-Orticoni, R. Haser, M. Czjzek, A. Makarov, M. Bruschi, Key role of phenylalanine 20 in cytochrome c_3: structure, stability, and function studies, Biochemistry 38 (1999) 33–41.
[39] L.M. Saraiva, C.A. Salgueiro, J. LeGall, W.M. Van Dongen, A.V. Xavier, Site-directed mutagenesis of a phenylalanine residue strictly conserved in cytochromes c_3, J. Biol. Inorg. Chem. 1 (1996) 542–550.
[40] Y. Takayama, E. Harada, R. Kobayashi, K. Ozawa, H. Akutsu, Roles of noncoordinated aromatic residues in redox regulation of cytochrome c_3 from *Desulfovibrio vulgaris* Miyazaki F, Biochemistry 43 (2004) 10859–10866.
[41] P.R. Pokkuluri, Y.Y. Londer, X. Yang, N.E. Duke, J. Erickson, V. Orshonsky, G. Johnson, M. Schiffer, Structural characterization of a family of cytochromes c_7 involved in Fe(III) respiration by *Geobacter sulfurreducens*, Biochim. Biophys. Acta 1797 (2010) 222–232.